Reconfigurable Three-Mode Converter Based on Cascaded Electro-Optic Long-Period Gratings

Jin, Wei; Chiang, Kin Seng

Published in:
IEEE Journal on Selected Topics in Quantum Electronics

Published: 01/09/2020

Document Version:
Post-print, also known as Accepted Author Manuscript, Peer-reviewed or Author Final version

Published version (DOI):
10.1109/JSTQE.2020.2969568

Publication details:
Jin, W., & Chiang, K. S. (2020). Reconfigurable Three-Mode Converter Based on Cascaded Electro-Optic Long-Period Gratings. *IEEE Journal on Selected Topics in Quantum Electronics*, *26*(5), Article 4500906. https://doi.org/10.1109/JSTQE.2020.2969568

Jin, W., & Chiang, K. S. (2020). Reconfigurable Three-Mode Converter Based on Cascaded Electro-Optic Long-Period Gratings. IEEE Journal on Selected Topics in Quantum Electronics, 26(5), [4500906]. https://doi.org/10.1109/JSTQE.2020.2969568.

Reconfigurable Three-Mode Converter Based on Cascaded Electro-Optic Long-Period Gratings

Wei Jin and Kin Seng Chiang, *Senior Member, IEEE*

***Abstract*—We propose an optical waveguide switch to realize complete reconfigurable mode conversion for three spatial modes. This device consists of three cascaded long-period grating mode converters of different types integrated along a three-mode lithium-niobate ($LiNbO_3$) waveguide, where the gratings can be electro-optically controlled to activate mode conversion independently. We fabricate the device with *z*-cut $LiNbO_3$, which employs graphene electrodes to drive the gratings and an electrode heater to achieve wavelength matching for the three gratings. The half-π voltages of the three gratings in a typical fabricated device, which is 26 mm long and operates at 1545 nm, are 48, 37, and 43 V, respectively. The proposed mode switch could find applications in reconfigurable mode-division-multiplexing communication systems based on few-mode fibers and other areas where programmable mode conversion is required.**

***Index Terms*—Electro-optic devices, gratings, integrated optics devices, multiplexing, optical switches, optical waveguide components.**

I. Introduction

Conversion between spatial modes of a few-mode optical fiber or waveguide is a subject that has attracted much research interest in recent years for its important applications in mode-division multiplexing (MDM) optical communication [1], imaging [2], sensing [3], quantum computation [4], etc. A number of fixed mode converters based on bulk-optics components [5], [6], optical fibers [7]–[10], and optical waveguides [11]–[15] for the above applications have been reported. For applications where dynamic routing of modes is needed, such as in reconfigurable MDM communication networks, programmable mode converters, or mode switches, are required. Various mode switches based on the thermo-optic (TO) effect [16]–[24], the acousto-optic effect [25], and the electro-optic (EO) effect [26]–[28] have been demonstrated. These mode switches [16]–[28], however, operate only for two spatial modes and thus provide very limited switching functions. A polymer TO four-mode switch based on a three-dimensional Mach-Zehnder interferometer is available [29], but it can provide only four out of twelve mode-switching functions for four modes and the switching speed (several milliseconds) is limited by the TO effect. While complete mode-switching functions can be implemented by placing a single-mode spatial switch matrix between a mode multiplexer and a matching mode demultiplexer, the device architecture required is complex and the optical loss is likely to be high. Nonetheless, a silicon TO four-mode switch that can provide all twelve mode-switching functions has been demonstrated with such an approach recently [30]. There are, however, few reports of EO mode switches that operate for three or more spatial modes. In this paper, we present an EO mode switch that can provide complete mode-switching functions for three spatial modes. Our device is based on integrating three cascaded EO-induced long-period gratings along a three-mode lithium-niobate (LiNbO3) waveguide. In principle, our approach can be scaled to handle more modes by increasing the number of gratings.

The structure of a long-period grating has been used for realizing mode converters in fibers [7]–[10], [31] and waveguides [12]–[15], [20], [27], [28]. By cascading a surface grating and a sidewall grating along a polymer waveguide, fixed three-mode and four-mode converters have also been demonstrated [15]. The reconfigurable mode converter considered in the present study consists of three cascaded long-period gratings of different types induced by the EO effect in a *z*-cut $LiNbO_3$ waveguide. The gratings near the two ends of the waveguide are designed to convert between the TM_{00} and TM_{10} modes and the grating in the middle is designed to convert between the TM_{00} and TM_{01} modes. With this structure, all the six mode-switching functions available with the three modes can be achieved. We fabricate the device by the proton-exchange process followed by annealing, which is the most popular fabrication process for commercial $LiNbO_3$ waveguide devices [32]. We use graphene as the material for the grating electrodes, which are placed directly on the waveguide surface. The use of graphene electrodes can do away with the buffer layer traditionally needed to isolate the electrodes from the waveguide, and hence reduce the driving voltage of the grating [27]. In addition, an electrode heater is deposited onto the middle grating to provide thermal tuning of the resonance wavelength of the grating, in case there is a need to compensate for any mismatch between the resonance wavelengths of the two types of gratings. For a typical fabricated device, which is 26 mm long and operates at 1545 nm, the half-π voltages of the three gratings are 48, 37, and 43 V, respectively, and the corresponding contrasts are higher than

Manuscript received November xx, 2019; revised xx, 2020; accepted xx, 2020. Date of publication xx, 2020; date of current version xx, 2020. This work was supported by Research Grants Council, University Grants Committee (RGC, UGC), Hong Kong under Project CityU 11205715. (Corresponding author: Kin Seng Chiang) The authors are with the Department of Electrical Engineering, City University of Hong Kong, 83 Tat Chee Avenue, Kowloon Tong, Hong Kong, China (e-mail: weijin@cityu.edu.hk; eeksc@cityu.edu.hk;).

This article has been accepted for publication in a future issue of this journal, but has not been fully edited. Content may change prior to final publication. Citation information: DOI 10.1109/JSTQE.2020.2969568, IEEE Journal of Selected Topics in Quantum Electronics

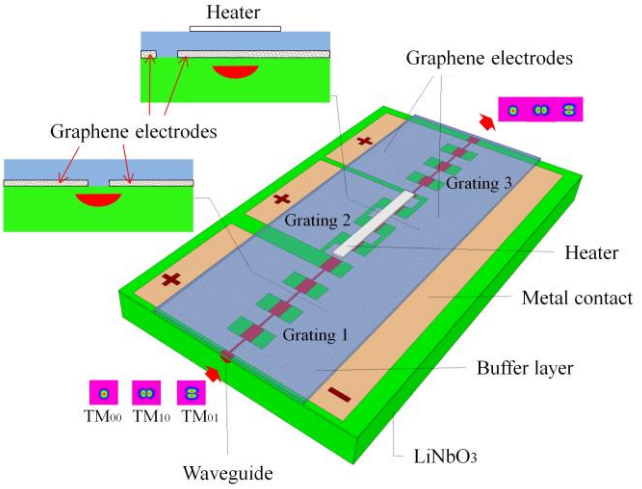

Fig. 1. Schematic diagrams of the proposed $LiNbO_3$ three-mode switch and the electrode configurations of Grating 1 (Grating 3) and Grating 2.

20 dB. The use of the EO effect in $LiNbO_3$ can provide a high switching speed limited only by the lengths of the gratings (~100 ps).

II. Device Structure and Operation Principle

Figure 1 shows a schematic diagram of the proposed mode switch, which consists of three cascaded EO long-period gratings (Grating 1, Grating 2, and Grating 3) integrated along a *z*-cut $LiNbO_3$ three-mode waveguide fabricated by the proton-exchange process. As the fabrication process increases only the extra-ordinary refractive index of the $LiNbO_3$ crystal, the resultant waveguide supports only the TM-polarized modes, in this case, the TM_{00}, TM_{10}, and TM_{01} modes, which correspond, respectively, to the LP_{01}, LP_{11a}, and LP_{11b} modes of an optical fiber. These modes have dominant electric-field components in the direction perpendicular to the waveguide surface and their power distributions are also shown in Fig. 1. The gratings near the two ends, i.e., Grating 1 and Grating 3, are identical and they are designed to achieve switching between the TM_{00} and TM_{10} modes, while the grating in the middle, i.e., Grating 2, is designed to achieve switching between the TM_{00} and TM_{01} modes. These two types of gratings require different electrode configurations, as shown in Fig. 1. To generate the periodic index modulations required for mode switching through the EO effect in $LiNbO_3$, three sets of periodic graphene electrodes are directly deposited on the surface of the waveguide and voltages are applied to the electrodes independently through the respective metal contacts.

For a long-period grating, the wavelength at which the mode-conversion effect is the strongest, i.e., the resonance wavelength, is determined by the phase-matching condition [27], [28]:

$$\lambda_0 = (N_1 - N_2)\Lambda \tag{1}$$

where N_1 and N_2 are the effective indices of the two coupled modes, respectively, and Λ is the pitch of the grating. The strength of the mode-conversion process, which depends on EO-induced refractive index change in the area where the two modes overlap, increases with the voltage applied to the

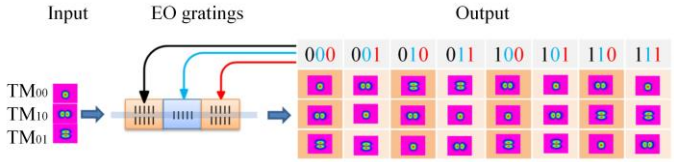

Fig. 2. Mode-switching matrix of the proposed mode switch, which covers all the six mode-switching functions available with three modes.

electrodes. The voltage at which one mode is completely coupled to the other mode is referred to as the half-π voltage. A driving voltage beyond the half-π voltage causes over-coupling (i.e., the converted mode is coupled back to the original mode) and lowers the mode-conversion ratio. Therefore, by switching the driving voltage from 0 V to the half-π voltage, one mode can be completely switched to the other mode. The use of graphene electrodes can exempt the need of putting a buffer layer between the waveguide and the electrodes and thus significantly reduce the half-π voltage [27].

For Grating 1 and Grating 3, a push-pull periodic electrode configuration, as shown in Fig. 1, is employed to exploit the largest EO coefficient r_{33} of the $LiNbO_3$ crystal, where the positive and negative electrodes are placed symmetrically on the waveguide surface and separated by a small gap along the central axis of the waveguide [27]. When a voltage is applied across the electrodes, one side of the waveguide experiences an increase in the refractive index, while the other side experiences a decrease. The resultant anti-symmetric EO-induced index distribution in the horizontal direction is coherent with the anti-symmetric distribution of the overlapped field of the TM_{00} and TM_{10} modes, which thus allows the coupling between the two modes.

For Grating 2, a periodic interdigitated electrode configuration, as shown in Fig. 1, is employed to generate the EO grating [28]. Because both the TM_{00} and the TM_{01} mode have symmetric field distributions in the horizontal direction, the EO-induced refractive-index change should also have a symmetric distribution in the horizontal direction to optimize the EO effect. An additional metal electrode heater with a buffer layer is placed on top to provide thermal tuning of the resonance wavelength to match that of Grating 1 and Grating 3.

With the three cascaded gratings, all the switching functions available with the three modes can be achieved. The mode-switching matrix of the device is shown in Fig. 2, where the three binary digits in each column of the table specify the states of the three EO gratings, respectively, with "1" and "0" referring to the "on" state (at the half-π voltage) and the "off" state (at 0 V), respectively. For the state "000", all the three gratings are turned off, the output mode is the same as the input mode. For the state "001", where Grating 1 and Grating 2 are off and Grating 3 is on, the TM_{00} and TM_{10} modes are converted to each other with the TM_{01} mode staying unchanged. The same function can be achieved with the state "100", where only Grating 1 is turned on. For the state "010", where only Grating 2 is on, the TM_{00} and TM_{01} modes are converted to each other with the TM_{10} mode staying unchanged. For the state "110", where Grating 1 and Grating 2 are on and Grating 3 is off, the input TM_{00} mode is converted

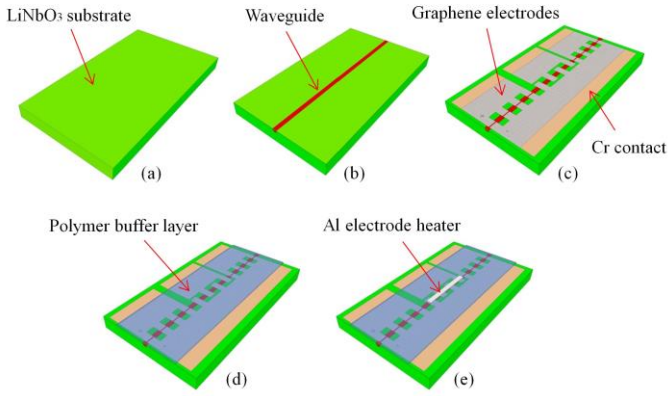

Fig. 3. Steps for the fabrication of the device: (a) preparation of $LiNbO_3$ substrate; (b) forming of waveguide by proton exchange followed by annealing; (c) transferring and patterning of graphene electrodes and formation of Cr contacts; (d) deposition of polymer buffer layer; and (f) deposition of Al electrode heater.

into the TM_{10} mode by Grating 1 and then passes through Grating 2 and Grating 3 without change, while the input TM_{10} mode is first converted to the TM_{00} mode and then further converted into the TM_{01} mode by Grating 2, and, similarly, the input TM_{01} mode passes through Grating 1 without change and then converted into the TM_{00} mode by Grating 2. Similar descriptions can be applied to the states "110", "101", and "111". As shown in Fig. 2, the eight states of the EO gratings, as represented by the combinations of three binary digits, cover all the six mode-switching functions available with the three modes, where two sets of states are duplicated ("000" and "101"; "001" and "100").

III. Device Fabrication

We fabricated the device with the process illustrated in Fig. 3 using our in-house microfabrication facilities. As illustrated in Fig. 3(a), we started with a *z*-cut, *y*-propagation $LiNbO_3$ substrate, which was 32 mm long, 12 mm wide, and 0.5 mm thick. We first deposited a chromium (Cr) thin film onto the substrate and formed a set of 6.0-μm wide strip openings on the Cr film by photolithography. We then put the sample into melted stearic acid for 16 h at 210 °C for proton exchange and removed the Cr mask afterwards. To recover the EO coefficient of the $LiNbO_3$ waveguide after proton exchange, we put the sample in an oven at 350 °C for 5 h for annealing and then into melted lithium stearic at 300 °C for 16 h for reverse proton exchange. The waveguide formed in this step is illustrated in Fig. 3(b). The core size of the waveguide was approximately 6.0 μm × 10.0 μm. The effective indices of the TM_{00}, TM_{01}, and TM_{10} modes of the waveguide, measured at 1536 nm with a prism-coupler system (Metricon2010) [33], were 2.16109, 2.15279, and 2.13957, respectively. We next polished both ends of the waveguide for input and output light coupling. The total length of the waveguide was 26 mm.

According to the measured effective indices of the three modes, we determined the pitches of the gratings from Eq. (1). The results were 186 μm for Grating 1 and Grating 3 and 72 μm for Grating 2 at the resonance wavelength ~1550 nm. The lengths of Grating 1, Grating 2, and Grating 3 were 5.0, 9.0, and 5.0 mm, respectively, and the duty cycles of the gratings were 50%. The gap distance between the positive and negative electrodes for Grating 2 was 2.0 μm.

We fabricated the graphene electrodes by first transferring a mono-layer graphene film onto the waveguide sample and then patterning it into the desired grating structures. The graphene film came with a PMMA buffer (Hefei Vigon Tech.), which had a dimension of 20 mm × 10 mm. We submerged the PMMA-attached graphene film in deionized water and fished it with the $LiNbO_3$ waveguide sample. After drying the sample, we removed the PMMA buffer with acetone and left the graphene film on the surface of the sample. We next spin-coated a photoresist thin film onto the graphene film and etched it into the desired grating pattern by photolithography. We then transferred the photoresist pattern to the graphene film by applying reactive-ion etching (RIE) in oxygen gas. We removed the remaining photoresist and deposited four Cr contact pads onto the sample. The waveguide with patterned graphene electrodes and Cr contact pads is illustrated in Fig. 3(c).

To provide a mechanism to align the resonance wavelengths of the gratings, we placed an electrode heater on Grating 2 to control its temperature and hence its resonance wavelength. According to our previous studies of $LiNbO_3$ waveguide gratings, the resonance wavelength of the TM_{00}–TM_{01} mode converter (Grating 1 and Grating 3) is insensitive to the temperature [28], while that of the TM_{00}–TM_{10} mode converter (Grating 2) is sensitive to the temperature [27], which justifies the use of thermal control for Grating 2 only. To fabricate the electrode heater, we first spin-coated a thin film of polymer to a thickness of 3 μm as a buffer layer on top of the graphene electrodes, as shown in Fig. 3(d). We then deposited and patterned an aluminum (Al) thin-film electrode to the desired shape by photolithography, as shown in Fig. 3(e). The Al heater had a width of 20 μm (which was large enough to fully cover the waveguide width), a thickness of ~100 nm, and a length of 9.0 mm (the same length of Grating 2). Finally, the edges of the polymer buffer layer were etched away to expose the four Cr contact pads for electrical connection.

A photo of the whole sample taken after patterning the graphene electrodes is shown in Fig. 4(a). The enlarged microscopic images of Grating 3 and Grating 2 are shown in Fig. 4(b)-(c) and Fig. 4(d)-(e), respectively. An image of the sample taken after the removal of photoresist and the deposition of Cr contact pads is shown in Fig. 4(f). Because the graphene film is almost transparent, it does not show up clearly in the microscopic image. For this reason, we drew some black lines on the back of the sample to roughly mark the area of the graphene electrodes, as shown in Fig. 4(f).

This article has been accepted for publication in a future issue of this journal, but has not been fully edited. Content may change prior to final publication. Citation information: DOI 10.1109/JSTQE.2020.2969568, IEEE Journal of Selected Topics in Quantum Electronics

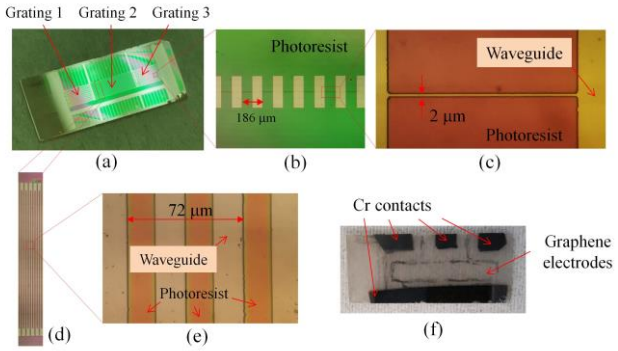

Fig. 4. (a) Photo of the whole sample taken after patterning the graphene electrodes, showing Grating 1, Grating 2, and Grating 3; (b) image of Grating 3, showing the grating pitch; (c) enlarged image of Grating 3, showing the gap of the electrodes; (d) image of Grating 2; (e) enlarged image of Grating 2, showing the grating pitch; and (f) image of the whole sample taken after removal of photoresist and deposition of Cr contact pads, where the black lines that mark the area of the graphene electrodes are drawn on the back of the sample.

IV. Device Characterization

We first characterized the performances of the individual gratings in the fabricated device. We launched only the TM_{00} mode into the device with a broadband source (SuperK COMPACT) and measured its output transmission spectra with an optical spectrum analyzer (Agilent 86140B) at different voltages applied to the gratings. Lensed single-mode fibers were used at both ends of the device to launch and collect light. We adjusted the lensed fibers at both ends to obtain the largest possible rejection band for the TM_{00} mode. The normalized transmission spectra measured at different voltages applied to the individual gratings are shown in Fig. 5(a)-(c). For Grating 1, a rejection band centered at ~1545 nm grows as the applied voltage increases, and reaches a maximum contrast at ~48 V, as shown in Fig. 5(a). A further increase in the applied voltage reduces the contrast of the rejection band due to over-coupling. The transmission characteristics of Grating 3 are similar to those of Grating 1, except for a small difference in the half-π voltage and the resonance wavelength, which, we believe, was due to the non-uniformity of the waveguide. As shown in Fig. 5(b), the half-π voltage of Grating 3 is ~43 V. For Grating 2, the resonance wavelength is ~1532 nm and the half-π voltage is ~32 V, as shown in Fig. 5(c). We also measured the near-field images of the output light from the device with a tunable semiconductor laser (KEYSIGHT) and an infrared camera (HAMAMATSU C2714). The results are shown as insets in Fig. 5(a)-(c). These images prove that the Grating 1 and Grating 3 indeed operate as TM_{00}-TM_{10} mode switches, while Grating 2 as a TM_{00}-TM_{01} mode switch, as expected. As shown in Fig. 5(a)-(c), there is a significant mismatch between the resonance wavelengths of Grating 1 (Grating 3) and Grating 2. To compensate for the wavelength mismatch, we applied electric power to the heater deposited on Grating 2. Figure 5(d) shows the normalized transmission spectra of Grating 2 measured at different heating powers (and at the corresponding half-π voltages) and Fig. 5(e) shows the variations of the resonance

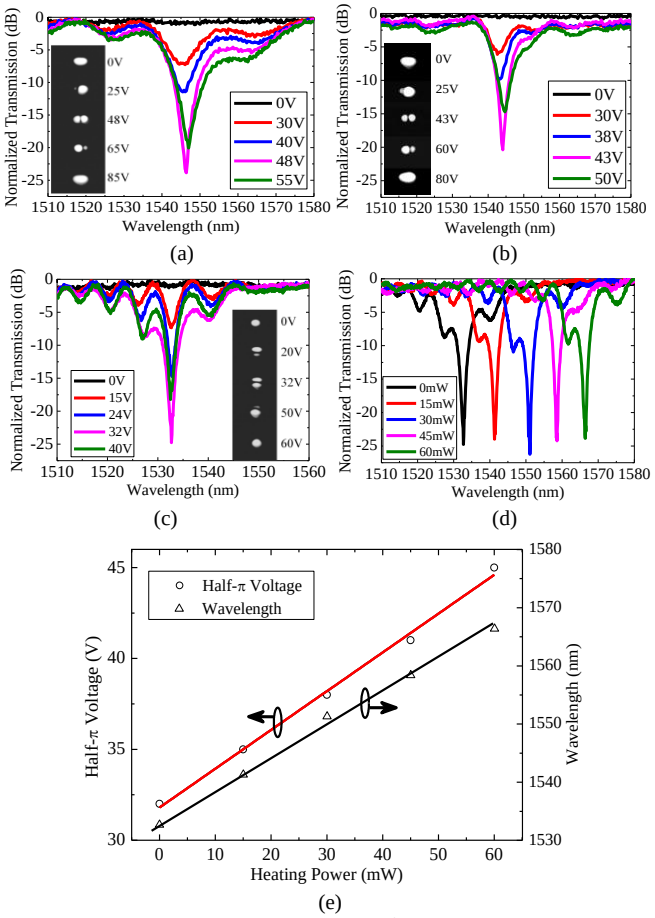

Fig. 5. Normalized transmission spectra of the TM_{00} mode measured at different driving voltages for (a) Grating 1, (b) Grating 3, and (c) Grating 2, respectively, when only the TM_{00} mode is launched into the device, where the insets show the near-field images of the output light obtained at different driving voltages. (d) Normalized transmission spectra of the TM_{00} mode for Grating 2 measured at different heating powers and the corresponding half-π voltages. (f) Variations of the half-π voltage and the resonance wavelength with the heating power for Grating 2.

wavelength and the half-π voltage with the heating power. As shown in Fig. 5(e), the resonance wavelength of Grating 2 reaches 1545 nm at a heating power of ~20 mW and the corresponding half-π voltage is 37 V. Therefore, the three gratings have matched resonance wavelengths at ~1545 nm when the heating power is ~20 mW. The mode-conversion ratios of the three gratings can be estimated from the contrasts of the rejection bands. As shown in Fig. 5, the strengths of the three gratings at ~1545 nm are higher than 20 dB measured at the respective half-π voltages, which corresponds to mode-conversion ratios higher than 99%. The propagation loss of the TM_{00} mode measured at 1550 nm is ~0.8 dB/cm.

We next measured the mode-switching functions of the device at different switching states. We applied an electric power of 20 mW to the electrode heater to ensure that the three gratings operated at the same resonance wavelength (1545 nm). Without applying any voltages to the gratings, we launched light into the device from the tunable laser (set at 1545 nm) and selectively excited the TM_{00}, TM_{10}, and TM_{01} mode individually by carefully adjusting the tilt angle and the position of the input lensed fiber in relation to the waveguide

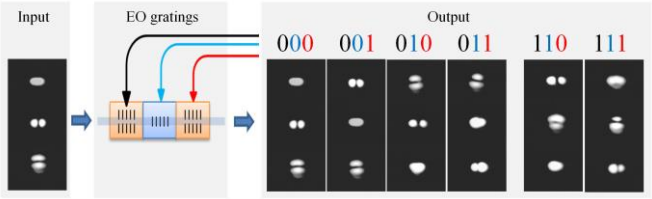

Fig. 6. Output near-field images of the device obtained at different switching states at 1545 nm, which cover all the six mode-switching functions available with three modes.

with a micro-positioner [34]. The output near-field images of these modes are shown in Fig. 6 as the input modes. We then applied the respective half-π voltages to Grating 1 (48 V), Grating 2 (37 V), and Grating 3 (43 V) to turn them on independently. The output near-field images of the device obtained at different switching states of the gratings are shown in Fig. 6, where the binary digits "1" and "0" represent the "on" and "off" states of each grating, respectively, in the same sense as that for Fig. 2. These results confirm that the device can achieve complete mode-switching functions for the three modes.

Theoretically, each grating can achieve 100% mode conversion at its resonance wavelength and the mode-conversion ratios in all the switching states can reach 100% if the resonance wavelengths of the three gratings are identical. The mode-conversion ratios achieved in our experiments (~99%) are limited by the uncertainties in the control of the driving voltages, the matching of the resonance wavelengths, and the uniformities of the waveguides. The performance of our mode switch could be further improved by refining the fabrication process.

V. Conclusion

We have proposed and experimentally demonstrated a three-mode switch based on the structure of three cascaded EO long-period gratings integrated along a $LiNbO_3$ waveguide, where the first and the last grating are identical TM_{00}-TM_{10} mode switches and the middle grating is a TM_{00}-TM_{01} mode switch. The device can provide all the six mode-switching functions available with three modes. Our experimental device fabricated by annealed proton exchange with *z*-cut $LiNbO_3$ has a total length of 26 mm, which employs patterned graphene electrodes to drive the grating switches and a metal electrode heater to compensate for the wavelength mismatch between the gratings. The half-π voltages of the three EO gratings are 48, 37, and 43 V, respectively, and the maximum mode-conversion ratios of the gratings at ~1545 nm are higher than 20 dB (or 99%). The bandwidth of our device is narrow. It should be possible to design broadband mode switches by using special grating profiles, such as length-apodized grating profiles [13]. With broadband grating designs, wavelength mismatch between gratings becomes less of a problem and thermal tuning of the resonance wavelength may be waived. The structure of the device is scalable in principle. For example, by cascading five, seven, and ten EO gratings, four-mode, five-mode, and six-mode switches could be realized, respectively. To overcome the length constraint of conventional low-index-contrast $LiNbO_3$ waveguides, our design approach may be applied to high-index-contrast $LiNbO_3$ waveguide platforms based on single-crystal $LiNbO_3$ thin films [35]. Our mode switch, when connected to a passive mode demultiplexer, can function as a switchable mode router, which could find important applications in reconfigurable MDM communication networks that require programmable mode routing.

References

[1] T. Mizuno and Y. Miyamoto, "High-capacity dense space division multiplexing transmission," *Opt. Fiber Technol.*, vol. 35, pp. 108–117, 2017.

[2] Y. Zhou *et al.*, "Quantum-limited estimation of the axial separation of two incoherent point sources," *Optica*, vol. 6, no. 5, p. 534, May 2019.

[3] P. Measor, S. Kühn, E. J. Lunt, B. S. Phillips, A. R. Hawkins, and H. Schmidt, "Multi-mode mitigation in an optofluidic chip for particle manipulation and sensing," *Opt. Express*, vol. 17, no. 26, pp. 24342–24348, Dec. 2009.

[4] J. Fu, "Quantum computations with optical waveguide modes," in *Proc. SPIE 5105 Quantum Information and Computation*, 2003, vol. 5105, pp. 225–233.

[5] R. Ryf *et al.*, "Mode-division multiplexing over 96 km of few-mode fiber using coherent 6 × 6 MIMO processing," *J. Lightw. Technol.*, vol. 30, no. 4, pp. 521–531, Feb. 2012.

[6] V. A. J. M. Sleiffer *et al.*, "737 Tb/s (96 x 3 x 256-Gb/s) mode-division-multiplexed DP-16QAM transmission with inline MM-EDFA," *Opt. Express*, vol. 20, no. 26, p. B428, Dec. 2012.

[7] C. D. Poole, H. M. Presby, and J. P. Meester, "Two-mode fibre spatial-mode converter using periodic core deformation," *Electron. Lett.*, vol. 30, no. 17, pp. 1437–1438, Aug. 1994..

[8] S. Ramachandran, Z. Wang, and M. Yan, "Bandwidth control of long-period grating-based mode converters in few-mode fibers," *Opt. Lett.*, vol. 27, no. 9, p. 698, May 2002.

[9] I. Giles, A. Obeysekara, R. Chen, D. Giles, F. Poletti, and D. Richardson, "Fiber LPG mode converters and mode selection technique for multimode SDM," *IEEE Photon. Technol. Lett.*, vol. 24, no. 21, pp. 1922–1925, Nov. 2012.

[10] J. Dong and K. S. Chiang, "Temperature-insensitive mode converters with CO2-laser written long-period fiber gratings," *IEEE Photon. Technol. Lett.*, vol. 27, no. 9, pp.1006-1009, May 2015. .

[11] J. B. Driscoll, R. R. Grote, B. Souhan, J. I. Dadap, M. Lu, and R. M. Osgood, "Asymmetric Y junctions in silicon waveguides for on-chip mode-division multiplexing," *Opt. Lett.*, vol. 38, no. 11, pp. 1854–1856, Jun. 2013.

[12] Y. Yang, K. Chen, W. Jin, and K. S. Chiang, "Widely wavelength-tunable mode converter based on polymer waveguide grating," *IEEE Photon. Technol. Lett.*, vol. 27, no. 18, pp.1985-1988, Sept. 2015.

[13] W. Wang, J. Wu, K. Chen, W. Jin, and K. S. Chiang, "Ultra-broadband mode converters based on length-apodized long-period waveguide gratings," *Opt. Express*, vol. 25, no. 13, p. 14341, Jun. 2017.

[14] W. Jin and K. S. Chiang, "Three-dimensional long-period waveguide gratings for mode-division-multiplexing applications," *Opt. Express*, vol. 26, no. 12, p. 15289, Jun. 2018.

[15] W. Jin and K. S. Chiang, "Mode converters based on cascaded long-period waveguide gratings," *Opt. Lett.*, vol. 41, no. 13, p. 3130, Jul. 2016.

[16] R. B. Priti and O. Liboiron-Ladouceur, "A reconfigurable multimode demultiplexer/switch for mode-multiplexed silicon photonics interconnects," *IEEE J. Sel. Top. Quantum Electron.*, vol. 24, no. 6, pp. 1–10, Nov. 2018.

[17] K. Chen, J. Yan, S. He, and L. Liu, "Broadband optical switch for multiple spatial modes based on a silicon densely packed waveguide array," *Opt. Lett.*, vol. 44, no. 4, pp. 907–910, Feb. 2019.

[18] X. Wang, W. Jin, Z. Chang, and K. S. Chiang, "Buried graphene electrode heater for a polymer waveguide thermo-optic device," *Opt. Lett.*, vol. 44, no. 6, p. 1480, Mar. 2019.

[19] S. Wang *et al.*, "On-chip reconfigurable optical add-drop multiplexer for hybrid wavelength/mode-division-multiplexing systems," *Opt. Lett.*, vol. 42, no. 14, p. 2802, Jul. 2017.

[20] W. K. Zhao, J. Feng, K. X. Chen, and K. S. Chiang, "Reconfigurable broadband mode (de) multiplexer based on an integrated thermally induced long-period grating and asymmetric Y-junction," *Opt. Lett.*, vol. 43, no. 9, pp. 2082–2085, May 2018.
[21] T. Zhou, H. Jia, J. Ding, L. Zhang, X. Fu, and L. Yang, "On-chip broadband silicon thermo-optic 2 x 2 four-mode optical switch for optical space and local mode switching," *Opt. Express*, vol. 26, no. 7, pp. 8375–8384, Apr. 2018.
[22] Y. Gao *et al.*, "Thermo-optic mode switch based on an asymmetric Mach–Zehnder interferometer," *IEEE Photon. Technol. Lett.*, vol. 31, no. 11, pp. 861–864, Jun. 2019.
[23] J. Lu *et al.*, "Dynamic mode-switchable optical vortex beams using acousto-optic mode converter," *Opt. Lett.*, vol. 43, no. 23, pp. 5841–5844, Dec. 2018.
[24] C. Sun, Y. Yu, G. Chen, and X. Zhang, "Integrated switchable mode exchange for reconfigurable mode-multiplexing optical networks," *Opt. Lett.*, vol. 41, no. 14, p. 3257, Jul. 2016.
[25] Y. Xiong, R. B. Priti, and O. Liboiron-Ladouceur, "High-speed two-mode switch for mode-division multiplexing optical networks," *Optica*, vol. 4, no. 9, p. 1098, Sep. 2017.
[26] M. Zhang, K. Chen, W. Jin, and K. S. Chiang, "Electro-optic mode switch based on lithium-niobate Mach–Zehnder interferometer," *Appl. Opt.*, vol. 55, no. 16, pp. 4418–4422, Jun. 2016.
[27] Z. Chang, W. Jin, and K. S. Chiang, "Graphene electrodes for lithium-niobate electro-optic devices," *Opt. Lett.*, vol. 43, no. 8, p. 1718, Apr. 2018.
[28] W. Jin and K. S. Chiang, "Mode switch based on electro-optic long-period waveguide grating in lithium niobate," *Opt. Lett.*, vol. 40, no. 2, p. 237, Jan. 2015.
[29] Q. Huang, W. Jin, and K. S. Chiang, "Broadband mode switch based on a three-dimensional waveguide Mach–Zehnder interferometer," *Opt. Lett.*, vol. 42, no. 23, p. 4877, Dec. 2017.
[30] L. Yang *et al.*, "General architectures for on-chip optical space and mode switching," *Optica*, vol. 5, no. 2, pp. 180–187, 2018.
[31] H. Sakata, H. Sano, and T. Harada, "Tunable mode converter using electromagnet-induced long-period grating in two-mode fiber," *Opt. Fiber Technol.*, vol. 20, no. 3, pp. 224–227, 2014.
[32] L. Arizmendi, "Photonic applications of lithium niobate crystals," *Phys. Status Solidi A*, vol. 201, no. 2, pp. 253–283, 2004.
[33] K. S. Chiang and S. Y. Cheng, "Technique of applying the prism-coupler method for accurate measurement of the effective indices of channel waveguides," *Opt. Eng.*, vol. 47, no. 3, pp. 034601(1-4), Mar. 2008.
[34] K. T. Ahmmed, H. P. Chan, and B. Li, "Broadband high-order mode pass filter based on mode conversion," *Opt. Lett.*, vol. 42, no. 18, pp. 3686–3689, Sep. 2017.
[35] C. Wang *et al.*, "Integrated lithium niobate electro-optic modulators operating at CMOS-compatible voltages," *Nature*, vol. 562, no. 7725, pp. 101–104, 2018.

Wei Jin received the B.S. degree in applied physics from Northwestern Polytechnical University, Xi'an, China, the M.S. degree in optics from South China Normal University, Guangzhou, China, and the Ph.D. degree in electronic engineering from the City University of Hong Kong in 2009. Since April 2009, he has been a research staff member in the Department of Electrical Engineering, City University of Hong Kong.

His research interests include $LiNbO_3$ and polymer optical waveguide devices.

Kin Seng Chiang (M'94, SM'19) received the B.E. (Hons. I) and Ph.D. degrees in electrical engineering from the University of New South Wales, Sydney, N.S.W., Australia, in 1982 and 1986, respectively.

In 1986, he spent six months with the Department of Mathematics, Australian Defense Force Academy, Canberra, A.C.T., Australia. From 1986 to1993, he was with the Division of Applied Physics, Commonwealth Scientific and Industrial Research Organization, Sydney, N.S.W., Australia. From 1987 to 1988, he received a Japanese Government research award and spent six months at the Electrotechnical Laboratory, Tsukuba City, Japan. From 1992 to 1993, he worked concurrently for the Optical Fibre Technology Centre, University of Sydney. In August 1993, he joined the Department of Electrical Engineering, City University of Hong Kong, Kowloon Tong, Hong Kong, where he is a Chair Professor. From 2007 to 2010, he was concurrently a Chang Jiang Chair Professor of the University of Electronic Science and Technology of China (UESTC) and, from 2012 to 2017, he was associated with UESTC under the National Thousand Talents Program. He has published more than 550 papers on optical fiber/waveguide theory and modeling, fiber/waveguide characterization, fiber/waveguide devices, optical sensors, optical interconnect, and nonlinear guided-wave optics.

Dr. Chiang (M'94, SM'19) is a Fellow of the Optical Society (OSA), a member of the International Society for Optical Engineering (SPIE), and the Australian Optical Society. He received the Croucher Award for 2000–2001. He served as an Associate Editor of *Journal of Lightwave Technology* during 2009–2014, and is currently an editor of *Light: Science & Applications*.